Brief Analysis of Aliasing in Polar and Keystone Formats for Spotlight Synthetic Aperture Radar

Jerald L. Bauck*

October 18, 2019

Abstract

Keystone formatting [1] for spotlight synthetic aperture radar is an alternative to the popular polar format and reduces the computational burden of resampling the polar data to a rectangular grid before inverse Fourier transformation by a fast Fourier transform—the polar format algorithm. After a brief review of relevant geometry and signals including linear frequency modulation and stepped sines, it is shown how to convert a polar-format radar into a keystone-format radar. Reconstructions from simulated data in both formats are shown and the differing kinds of image aliasing are examined.

1 Introduction

SPOTLIGHT synthetic aperture radar is a microwave remote sensing scheme in which a radar on a stand-off moving platform emits structured pulses and collects the reflected energy as the antenna dwells on a spot on the ground as shown in Figure 1. Under some broad assumptions discussed below, an image of the reflectivity of the illuminated ground patch is formed by processing the reflected energy, the main step of the processing being inverse Fourier transformation.

It is common to assume that the emitted waves are planar over the ground patch and that the the variation in propagation attenuation over the ground patch is negligible. Both approximations tend to truth as the distance between the radar and the ground patch is large while the ground patch is small. Methods exist to compensate for nonplanar waves [2] and other methods exist to remove both approximations [3, 4, 5, 6].

Linear frequency modulation (LFM) is commonly used for the transmitted signal and a rough sketch of the signal processing of the received signals is, for each reflected pulse, to perform a mixing operation with a modified version of the transmitted signal [7] or a similar operation by matched filtering or de-chirping, treating these sampled discrete data as points particularly arrayed in the two-dimensional Fourier transform plane of the ground patch ("formatting"), and subsequently performing an inverse two-dimensional Fourier transform.

The most popular Fourier formatting is polar formatting.

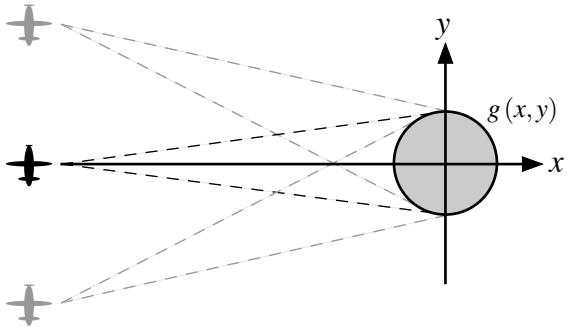

Figure 1: Collection geometry for spotlight synthetic aperture radar showing moving platform and ground patch to be imaged.

A less common format is keystone or trapezoidal formatting [1] which carries a significant advantage over polar formatting. Figure 2 shows these two formats schematically.

The purpose of this paper is to describe these two forms of Fourier formatting of spotlight SAR data, describe how to convert a polar-format radar into a keystone-format radar, and to study the differences in particular with respect to aliasing. In this service, two kinds of waveforms that approximate the LFM will be discussed and one used to create image reconstructions of a single small scatterer at the origin of the ground patch from both polar and keystone data, and then to describe in detail how image aliasing caused by sampling in the Fourier plane differs between the two formats. This knowledge can inform system design aspects that aim to tolerate or reduce the effects of aliasing.

2 Geometry and Waveforms

Many kinds of waveforms are used in radar including spotlight SAR. LFM is a popular SAR waveform because it has

*Originally published on October 18, 2019. Available at engrxiv.org. This paper has not been peer reviewed. Jerry Bauck welcomes comments and can be reached by e-mail at this address after left-shifting each alpha character by one position, e.g., f becomes e: kfssz@cbvdl.ofu.

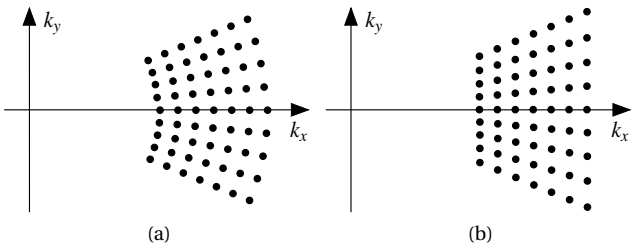

Figure 2: Sampling schemes of the Fourier transform of the ground patch $g(x,y)$ by (a) polar formatting and (b) keystone formatting.

many nice properties including, after demodulation, the mapping of range to frequency. A detailed analysis of LFM in spotlight SAR is offered in [7] wherein discrete polar samples of the Fourier plane appear. Other waveforms are suitable and stepped frequency or stepped sine signals [8, 9] will be considered herein for simplicity and clarity of exposition since they, too, provide discrete Fourier plane samples. Similar principles apply to other waveforms with perhaps some modifications in post-processing [10].

Define the ground patch as a complex-valued microwave reflectivity function on an x-y coordinate system, $g(x,y) = g(\mathbf{x})$. Ordinarily the support is assumed to be limited to a circle of a specified radius by the antenna pattern but that will have no bearing here. Let there be another coordinate system, the x'-y' system, sharing the same origin as the x-y system but rotated counterclockwise by an angle θ and with the radar at a distant point on the negative x' axis. In the rotated system the ground patch is $g'(x',y')' = g'(\mathbf{x}')'$ where the $'$ notation relates to rotated systems, axis variables, and functions defined thereon. Let the transmitter emit a harmonic signal of radian frequency ω, $e^{j\omega t}$. Under the plane wave assumption and with a unit scatterer at $\mathbf{x}_s$, this creates a reflected, backward-traveling field in the vicinity of the radar

$$r(x,y,t) = e^{j[\omega t + \mathbf{k}\cdot(\mathbf{x}-2\mathbf{x}_s)]} \tag{1}$$

after removing the bulk delay between receiver and $(0,0)$ and normalizing the propagation attenuation to one. Here, $|\mathbf{k}| = k$ and $\mathbf{k} = (k_x, k_y) = (k\cos\theta, k\sin\theta)$ is the propagation vector with wavenumber $k = \omega/c$ and c the speed of light. The receiving antenna acts to sample the field at a single point, generating the spatial phasor (remove $e^{j\omega t}$) receiver signal

$$r'_x(x') = e^{j(kx'-2\mathbf{k}\cdot\mathbf{x}_s)}. \tag{2}$$

(Reference [10] contains a full development from first principles of these basic results and others mentioned herein.) An important concept is that a harmonic illumination of the ground patch with transmitter signal $e^{j\omega t}$ samples its Fourier transform $G(\mathbf{k})$ at $G(2k\hat{\mathbf{x}}')$ where $\hat{\mathbf{x}}' = (\cos\theta, \sin\theta)$ is a unit vector in the direction of the x' and k_x axes. The plane can be sampled at arbitrary points by adjusting the angular position θ of the radar and the sinusoid frequency ω. Spotlight SAR functions to place many such samples of $G(\mathbf{k})$ over a limited region of the $\mathbf{k}$ plane and then to find an estimate of the bandlimited ground patch by Fourier inversion, either by the so-called direct Fourier inversion also known as the polar format algorithm (PFA) [2] or by backprojection [11, 10]. For example, backprojecting (2) reconstructs the phasor version of field (1); performing such backprojections from all θ and all ω reconstructs a Dirac impulse at $\mathbf{x}_s$. However, the usually preferred Fourier inversion method, the polar format algorithm, proceeds by interpolating the polar formatted data to a rectangular sampling grid and then inverting by using a fast Fourier transform (FFT). It is the ability to use an FFT that offers a computational advantage over backprojection that makes this preferable, although some architectures [11, 12] and algorithms [13] can reduce that advantage. Even so, the two-dimensional interpolation required by the polar format algorithm represents an additional computational stage, usually proceeding by two one-dimensional steps where the first step resamples the polar data along lines of constant θ, resulting in a format similar to Figure 2(b). The second one-dimensional interpolation is along lines parallel to the k_y axis in Figure 2(b) yielding the desired rectangular sampling grid.

A family of discrete-frequency, or stepped, sines, can produce the same constellation of polar samples in the Fourier plane as samples of demodulated LFM signals from discrete values of θ, even though some details differ which are not important here; inverting the constellation in either case is the same, however.

The process of generating keystone formatted data directly will be described shortly. It potentially somewhat increases the transmitter burden of synthesizing the transmitted signals which is the tradeoff for reducing the interpolation burden later. An additional advantage of generating keystone-formatted data directly is that the simpler interpolation stage should generate less error in the image.

There are two kinds of stepped sine waveforms. The first is sequentially stepped sines whereby a single pulse is divided into sub-pulses each of which is a sine segment with a frequency different than all the others. Let $f = \omega/2\pi$ be the cyclical temporal frequency and $\mathbf{l} = \mathbf{k}/2\pi = (l_x, l_y)$ the cyclical spatial propagation vector. Cyclic and radian quantities will be used as convenient, with similar notational accoutrements, without prejudice. With uniform amplitude, a waveform in which each sub-pulse has a higher frequency than the preceding sub-pulse, where the beginning frequency is $f_b = f_0$, the ending frequency is $f_e > f_b$, the number of frequencies and sub-pulses is N, $\Delta f = (f_e - f_b)/(N-1)$, and the sub-pulse length is T_p, is, along with its Fourier transform,

$$s(t) = \sum_{n=0}^{N-1} \mathrm{rect}\left(\frac{t-nT_p}{T_p}\right) e^{j2\pi(f_b+n\Delta f)(t-nT_p)}$$

$$S(f) = T_p \sum_{n=0}^{N-1} \mathrm{sinc}\left[(f-f_b-n\Delta f)\,T_p\right] e^{-j2\pi f T_p}$$

where $\mathrm{rect}(x)$ is unity for $|x| \le 1/2$ and zero otherwise and

$\mathrm{sinc}(x) = \sin(\pi x)/\pi x$. (A variation allows gaps between the sub-pulses.) Another kind of stepped-sine waveform is the stacked sine version whereby sines of all the discrete frequencies are transmitted simultaneously. With the pulse length T_p, the time- and frequency-domain signals are be

$$\begin{aligned} s(t) &= \mathrm{rect}\left(\frac{t}{T_p}\right) \sum_{n=0}^{N-1} e^{j2\pi(f_b + n\Delta f)t} \\ &= \mathrm{rect}\left(\frac{t}{T_p}\right) \frac{\sin\left(N\pi\Delta f\, t\right)}{\sin\left(\pi\Delta f\, t\right)} e^{j2\pi(f_b + \Delta f(N-1)/2)t} \end{aligned} \tag{3}$$

$$S(f) = T_p \sum_{n=0}^{N-1} \mathrm{sinc}\left[\left(f - f_b - n\Delta f\right) T_p\right].$$

The structure of the sequential and stacked sines differs in that the sequential sines, in both time and frequency domains, contain an extra phase term. In the frequency domain this term can cause vigorous interference between sinc lobes if Δf is too small or if T_p is too small; otherwise, the oscillations are partially limited by the sinc sidelobes and are further reduced in effect due to partial cancellation from phase terms of neighboring sinc sidelobes. For the stacked time-domain signal, if T_p is long enough, the various sines build nicely into the Dirichlet function $\sin(N\pi x)/\sin(\pi x)$ [14]. Either version will convey the salient points of this paper; since the stacked version is less complicated and easier to interpret it will be preferred here. The sines will be considered to be long enough to avoid significant lobing effects and ground patch edge effects. It is not the purpose of this paper to discuss differences in transmitter and receiver design or signal-to-noise ratio for the two types of stepped sines.

3 Polar-to-Keystone Format Mapping

Keystone formatting can be obtained by conceptually starting with a polar format. As seen in Figure 2, polar-format points in the plane are reduced in the l_x-direction by $\cos\theta$ relative to a point representing a wave propagating in the $\theta = 0$ direction; thus, if a new frequency $f' = f/\cos\theta$ and consequently $\mathbf{l}' = \mathbf{l}/\cos\theta$ are used, then the new sampling point is $(l, l\tan\theta)$ so that the first coordinate is constant for all θ. (Assume $|\theta| < \pi/2$.) When this adjustment is made to all relevant points in the 2D frequency domain, the keystone format is established. It is not necessary to retain the same set of angles when converting a polar plan to a keystone plan.

LFM waveforms for keystone format are readily obtained by adjusting the beginning frequency, ending frequency, and chirp rate [1]. Consider a prototype LFM signal, also suitable for $\theta = 0$,

$$s(t) = e^{j\pi\alpha t^2}$$

between t_b and t_e, $t_b < t_e$, and zero elsewhere. The instantaneous frequency $f_i(t) = d\phi/2\pi dt = \alpha t$, $f_i(t_b) = f_b = \alpha t_b$, $f_i(t_e) = f_e = \alpha t_e$, and $\alpha = \left(f_e - f_b\right)/(t_e - t_b)$. Adapting this signal to the keystone format, the parameters become functions of θ: $f'_b(\theta) = f_b/\cos\theta$, $f'_e(\theta) = f_e/\cos\theta$, and $\alpha'(\theta) = \left(f'_e(\theta) - f'_b(\theta)\right)/(t_e - t_b)$, the latter assuming that t_b and t_e are the same as the prototype. The frequency domain signal is shifted to the right and stretched[1]. The intention is that the prototype corresponds to $\theta = 0$ so that $f_b = f'_b(0)$ etc.

The same rule as derived in the previous paragraph can be applied to any signal $s(t)$ with frequency support between f_b and f_e—move the beginning point to f'_b and stretch the spectrum by a factor of $\beta = \left(f_e - f_b\right)/\left(f'_e - f'_b\right)$, that is, $S'(f) = S\left(\beta\left(f - f'_b + f_b\right)\right)$.

By now the adaptation to keystone format for a stepped sine signal should be obvious. For a collection of frequencies used for polar format at a particular angle θ, $\mathsf{F} = \left\{f_n = f_0 + n\Delta f,\ n \in 0, 1, \ldots N-1,\ f_0 = f_b,\ f_{N-1} = f_e\right\}$, define a new collection for keystone format as $\mathsf{F}' = \left\{f'_n = f_n/\cos\theta,\ n \in 0, 1, \ldots N-1,\ f'_0 = f'_b,\ f'_{N-1} = f'_e\right\}$.

4 Polar and Keystone Format Aliasing

To demonstrate the keystone waveform principle, several plane waves composed from stacked sines were summed over the simulated ground patch in the manner of Section §2 in the discussion of (1) and (2), mimicking the coherent summation that is normally done in the receiver. This method avoids all interpolation artifacts which is desirable since the present interest is not in interpolation studies but in aliasing artifacts specific to the format style. This was done for both polar and keystone formats using F and F' respectively. The ground patch is a square region ranging over ±50 spatial units on each side with the origin in the middle. There was no 1D interpolation in the backprojection because the backprojected functions are known exactly at all points. (This luxury is not available in an actual radar.) The summed field was computed over a 256×256 grid overlaid on the ground patch. There was no $\mathrm{rect}(\cdot)$ applied to the signals so the only windowing in effect is due to the ground patch limits. The scatterer position is in the middle, $\mathbf{x}_s = (0, 0)$. Angle θ ranged from $-30°$ to $+30°$ from 120 angles. Temporal frequencies ranged from $f_b = 2$ to $f_e = 6$; with $c = 10$, spatial frequencies for polar and prototype keystone signals ranged from $l_{xb} = 0.2$ to $l_{xe} = 0.6$. The number of stepped sine frequencies $N = 26$ so that $\Delta l_x = 0.016$. These are not typical radar parameters but they were chosen for expository purposes. The results are shown in Figure 3 where parts (b) and (d) are the frequency domain versions of parts (a) and (c) respectively, computed by a 2D DFT merely to confirm that the constituent plane waves are in fact from the expected formats.

(Each plane wave is represented as a near-impulse in the frequency plane. However, since they are not distributed uniformly, each impulse must be weighted according to how much area it represents. The Jacobian for polar format → rectangular format is of course frequency radius ρ; the Jacobian for keystone format → polar format is $\cos\theta$, and so

[1] Alternatively, the sample rate of the received baseband signal can be adjusted pulse-to-pulse [1, Section 3.4].

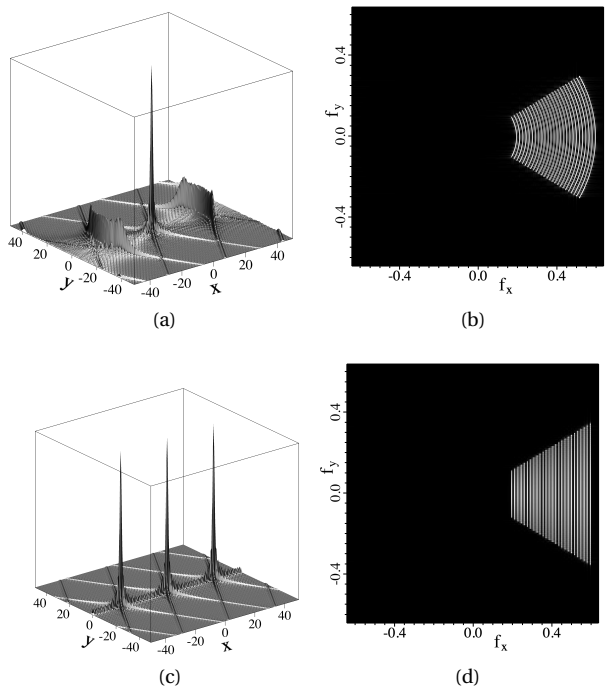

Figure 3: Impulse reconstructions and discrete Fourier transforms collected over a restricted range of look angles and signal bandwidth. (a) Impulse response from polar format data showing aliasing; (b) Discrete Fourier transform of (a); (c) Impulse response from keystone format data showing aliasing; (d) Discrete Fourier transform of (c).

the composite Jacobian needed here for correct weighting is $\rho\cos\theta$. The reason the mostly non-black parts of Figure 3(b) and (d) are relatively uniform is because each pixel of the image contains several impulses, thus computing a kind of graphical total which is nearly constant across pixels.)

Salient features of Figure 3 are sharp, well-defined central spikes for both polar and keystone impulse responses along with lower-level circular-arc ridges appearing in the polar spatial plot and aliased spikes in the keystone spatial plot—these artifacts were left in purposefully and will be discussed shortly.

4.1 Keystone Discussion

The keystone reconstruction shows several interesting features. If the same set of angles is used for both polar and keystone Fourier data, the area covered in the latter case is somewhat greater which likely would cause somewhat increased resolution. But for the same reason, the keystone format might result in under-sampling in the region of larger l_x and l_y due to sample points being farther apart. Taking this idea into the realm of DFT inversion to yield the image, the same phenomenon might cause wrap-around in the l_y-direction of the DFT that wasn't present in the polar version.

The keystone display of Figure 3(d) shows a periodic discrete structure in the l_x direction that is not present in the corresponding polar frequency plot of Figure 3(b), implying a periodic discrete structure in the image along the x axis which indeed appears in Figure 3(c). The l_x-period is $\Delta l_x = 0.016$ and thus the x-period is $1/2\,\Delta l_x = 31.25$ which is the spacing between spikes in Figure 3(c). (The 2 derives from two-way propagation and carries over from e.g. (1) or (2).) This implies a sample-rate maximum in Δl_x to avoid image aliasing in keystone-formatted data. Interpret $G(\mathbf{l})$ as a series of impulsive δ-ridges parallel to the l_y axis and apply the projection-slice theorem. A l_y-projection of $G(\mathbf{l})$,

$$\bar{G}_0(l_x) = \int_{-\infty}^{\infty} G(l_x, l_y)\, dl_y = \sum_{n=0}^{N-1} \delta(l_x - l_{xb} - n\Delta l_x)$$

the inverse Fourier transform of which is

$$\begin{aligned} \bar{g}_0(x) &= \sum_{n=0}^{N-1} \int_{-\infty}^{\infty} \delta(l_x - l_{xb} - n\Delta l_x)\, e^{j4\pi l_x x} dl_x \\ &= \sum_{n=0}^{N-1} e^{j4\pi x(l_{xb} + n\Delta l_x)} \\ &= \frac{\sin(2\pi N \Delta l_x x)}{\sin(2\pi \Delta l_x x)} e^{j4\pi(l_{xb} + \Delta l_x (N-1)/2)x} \end{aligned} \tag{4}$$

where the factor 2 has been attached to spatial variable x for round-trip travel. (The projection-slice theorem employs the direct Fourier transform; thus, $\bar{g}_0(x)$ expressed above is reversed in x compared to a central slice of $g(\mathbf{x})$.) When a spatial impulse response like Figure 3(c) is made but with plane waves extending in θ over 0° to 360° and a central slice is made at zero degrees and compared to (4), they are essentially identical. The periodicity is not a result of DFT processing but is the periodicity of the transmitted signal. The aliased spikes of Figure 3(c) will disappear if a rect(t/T_p) window is placed on the transmitted signal (3) such that $cT_p < 50$, the distance to the edge of the ground patch, or if Δl_x is decreased enough, to 0.01 in this case.

4.2 Polar Discussion

The circular-arc ridges in the polar image Figure 3(a) are the same distance from the origin as the spurious spikes in Figure 3(c). The real and imaginary parts of this image exhibit classic caustic formation but the fine details get lost in the magnitude plot of Figure 3(a). If the θ coverage is extended over 0° to 360°, the partial-angle ridges of Figure 3(a) develop into a full circle of ridges at the same radius.

The ridges of a full-circle simulation can be predicted with a bit of analysis. 2D Fourier transforms of circularly-symmetric functions such as a full-circle summation of plane waves of various frequencies mentioned immediately above reduce to a 1D transform of the radial variable in both domains, the Hankel transform [15]. Let the radial spatial variable be r and the radial frequency variable be ρ. A continuous-in-θ impulsive ring of radius a in the frequency domain is $\delta(\rho - a)$. The frequencies F are used so that there

are several δ-rings summed to make the symmetrical frequency domain field

$$H(\rho) = \sum_{n=0}^{N-1} \delta\left(\rho - l_{xb} - n\Delta l_x\right)$$

The Hankel transform of $\delta\left(\rho - a\right)$ is $2\pi a J_0\left(2\pi a r\right)$ so the spatial symmetric field for this collection of impulse rings is

$$h(r) = 2\pi \sum_{n=0}^{N-1} \left(l_{xb} + n\Delta l_x\right) J_0\left(4\pi\left(l_{xb} + n\Delta l_x\right) r\right).$$

As before, an excellent match is seen between $h(r)$ and a central image slice taken through a summation computed from 720 plane waves comprised of N spatial frequency components at $l_{xb} + n\Delta l_x$, $l_{xb} = 0.2$ and $l_{xe} = 0.6$.

In the polar spatial field there is an apparently infinite series of ring-shaped ridges at multiples of $1/2\,\Delta l_x$ as seen both in simulations and predicted by $h(r)$; the amplitude of each succeeding ridge is a little less than the previous one. Likewise, the spurious spikes in the keystone spatial function continue indefinitely along the x axis at multiples of $1/2\,\Delta l_x$.

5 Version History

- October 18, 2019. First published.

References

[1] A. W. Doerry, "Basics of polar-format algorithm for processing synthetic aperture radar images," Sandia National Laboratories, Albuquerque, New Mexico 87185 and Livermore, California 94550, Sandia Report SAND2012-3369, May 2012. [Online]. Available: www.ntis.gov

[2] W. G. Carrara, R. M. Majewski, and R. S. Goodman, *Spotlight Synthetic Aperture Radar: Signal Processing Algorithms*, ser. Artech House Remote Sensing Library. Boston: Artech House, 1995.

[3] J. L. Bauck and W. K. Jenkins, "Tomographic processing of spotlight-mode synthetic aperture radar signals with compensation for wavefront curvature," in *1988 International Conference on Acoustics, Speech, and Signal Processing, ICASSP-88*, vol. 2. New York: Institutue of Electrical and Electronics Engineers, April 1988, pp. 1192–1195.

[4] ——, "Convolution-backprojection image reconstruction for bistatic synthetic aperture radar," in *IEEE International Symposium on Circuits and Systems, 1989*. Portland, Oregon: Institutue of Electrical and Electronics Engineers, May 1989, pp. 1512–1515 vol.3.

[5] J. L. Bauck, "Tomographic processing of synthetic aperture radar signals for enhanced resolution," Ph.D. dissertation, Univrsity of Illinois at Urbana-Champaign, Urbana, Illinois, November 1989, [Online]. Available: Primary https://engrxiv.org/6a2tn/ or Secondary http://www.dtic.mil/docs/citations/ADA217178.

[6] J. L. Bauck and W. K. Jenkins, "Convolution-backprojection image reconstruction for bistatic synthetic aperture radar with correction for wavefront curvature and propagation attenuation," in *Millimeter Wave and Synthetic Aperture Radar*, vol. 1101. International Society for Optics and Photonics, 14 August 1989, pp. 11–18. [Online]. Available: https://doi.org/10.1117/12.960509

[7] D. C. Munson, J. D. O'Brien, and W. K. Jenkins, "A tomographic formulation of spotlight-mode synthetic aperture radar," *Proceedings of the IEEE*, vol. 71, no. 8, pp. 917–925, Aug 1983.

[8] B.-C. Wang, *Digital Signal Processing Techniques and Applications in Radar Image Processing*, ser. Information and Communications Technology Series. Hoboken, New Jersey: John Wiley & Sons, 2008.

[9] J. E. Luminati, "Wide-angle multistatic synthetic aperture radar: Focused image formation and aliasing artifact mitigation," DTIC Document, Tech. Rep., 2005.

[10] J. L. Bauck. (2019, October) A rationale for backprojection in spotlight synthetic aperture radar image formation. [Online]. Available: https://engrxiv.org/

[11] M. D. Desai, "A new method of synthetic aperture radar image reconstruction using modified convolution backprojection algorithm," Disertation, University of Illinois at Urbana-Champaign, Urbana, Illinois, 1985. [Online]. Available: https://apps.dtic.mil/dtic/tr/fulltext/u2/a170652.pdf

[12] A. Reigber, M. Jager, A. Dietzsch, R. Hansch, M. Weber, H. Przybyl, and P. Prats, "A distributed approach to efficient time-domain sar processing," in *2007 IEEE International Geoscience and Remote Sensing Symposium*, July 2007, pp. 582–585.

[13] S. Basu and Y. Bresler, "O(n/sup 2/log/sub 2/n) filtered backprojection reconstruction algorithm for tomography," *IEEE Transactions on Image Processing*, vol. 9, no. 10, pp. 1760–1773, Oct 2000. [Online]. Available: https://ieeexplore.ieee.org/document/869187

[14] R. E. Blahut, *Theory of Remote Image Formation.* Cambridge, United Kingdom: Cambridge University Press, 2004.

[15] R. N. Bracewell, *The Fourier Transform and its Applications*, 3rd ed. New York: McGraw-Hill, 2000.